Supporting Information

Heteroatom-Rich Porous Carbons Derived from Nontoxic Green Organic Crystals for High-Performance Symmetric and Asymmetric Supercapacitors with Aqueous/Gel Electrolyte

Meimei Wang [a], Kuihua Han [a, *], Jianhui Qi [a], Jinxiao Li [a], Zhaocai Teng [a], and Jigang Zhang [a]

[a] School of Energy and Power Engineering, Shandong University, Jinan, Shandong, 250061, China

[*] Corresponding author. E-mail: hankh@163.com (Kuihua Han)

Number of pages: 13
Number of Figures: 16
Number of Tables: 2

Preparation process of bagasse pith-derived porous carbon

Sugarcane were purchased from market. Cleaned cane stalk was peeled to obtain sugarcane pith. Sugarcane juice from the sugarcane pith was pressed out, and bagasse pith was obtained. The bagasse pith was washed repeatedly with deionized water, and dried at 120 °C for a week in a blast drying oven. The dried bagasse pith was crushed, and bagasse pith powder was sifted with a standard sieve with a aperture of 0.2 mm. Bagasse pith-derived porous carbon was prepared with bagasse pith powder as precursor, and the following preparation process was the same as that of the heteroatom-rich porous carbons in the paper.

Table S1. Elemental contents of L-lysine, L-tyrosine, L-histidine, glucose and sucrose.

Sample	C (wt%)	N (wt%)	O (wt%)	H (wt%)
L-lysine	49.32	19.18	21.92	9.59
L-tyrosine	59.67	7.73	26.52	6.08
L-histidine	46.45	27.10	20.65	5.81
Glucose	40.00	—	53.33	6.67
Sucrose	42.11	—	51.46	6.43

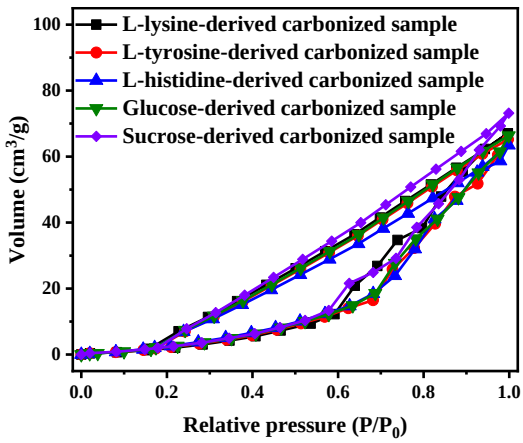

Figure S1. N_2 adsorption-desorption isotherms of the carbonized samples.

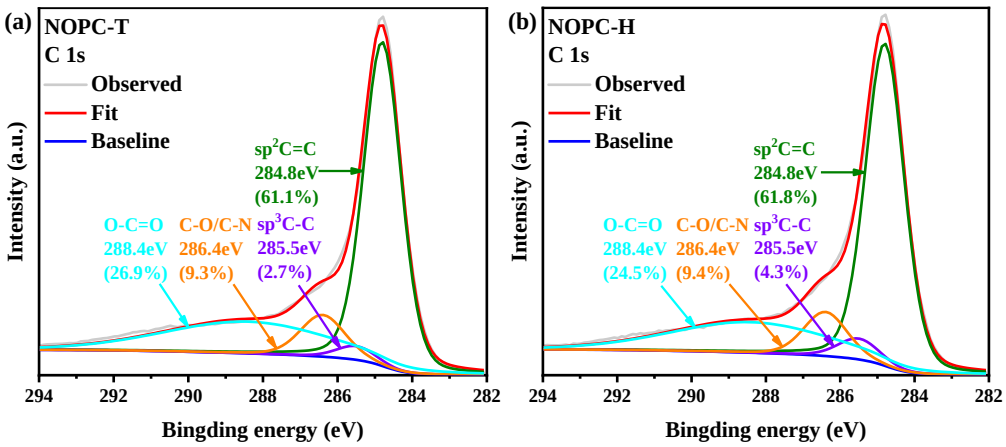

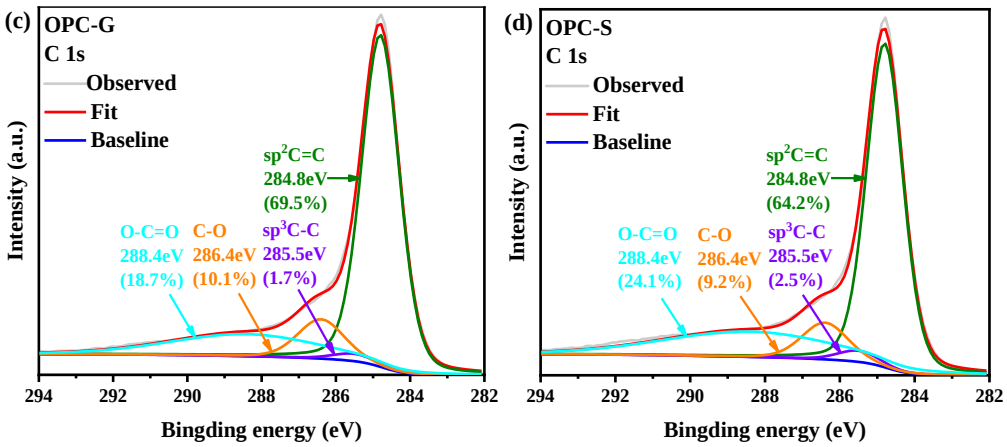

Figure S2. C 1s XPS spectra of (a) NOPC-T, (b) NOPC-H, (c) OPC-G and (d) OPC-S.

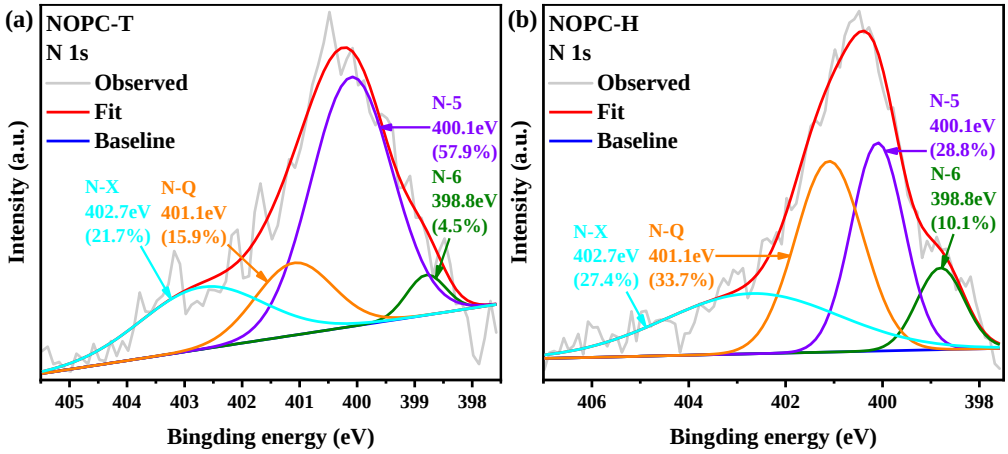

Figure S3. N 1s XPS spectra of (a) NOPC-T and (b) NOPC-H.

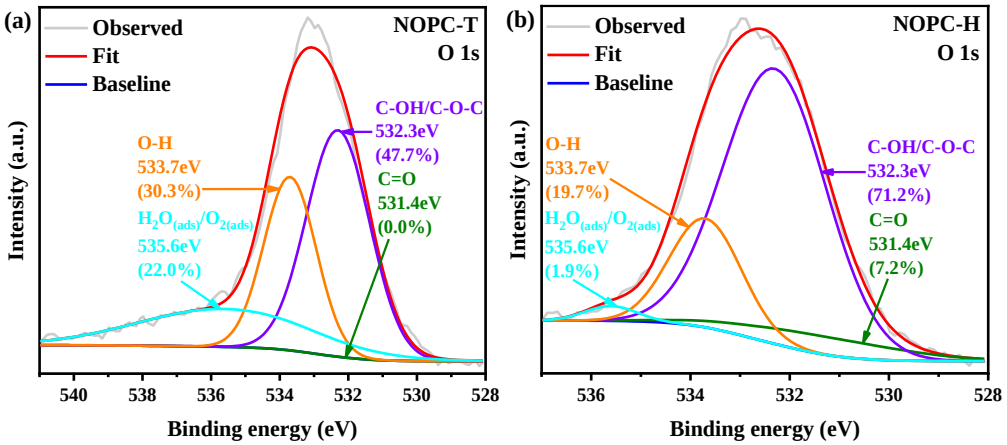

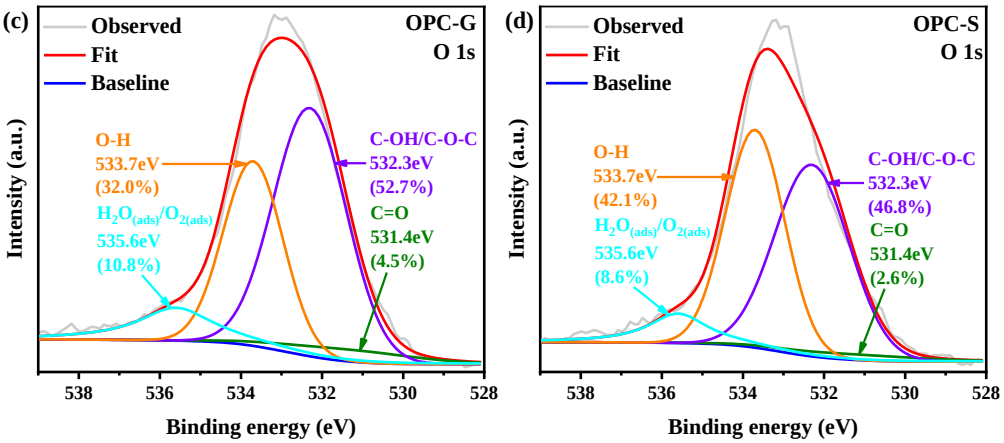

Figure S4. O 1s XPS spectra of (a) NOPC-T, (b) NOPC-H, (c) OPC-G and (d) OPC-S.

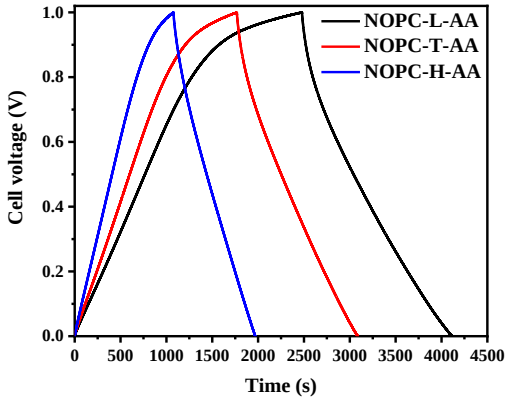

Figure S5. GCD curves of NOPC-L-AA, NOPC-T-AA and NOPC-H-AA at 0.1 A g^{-1}.

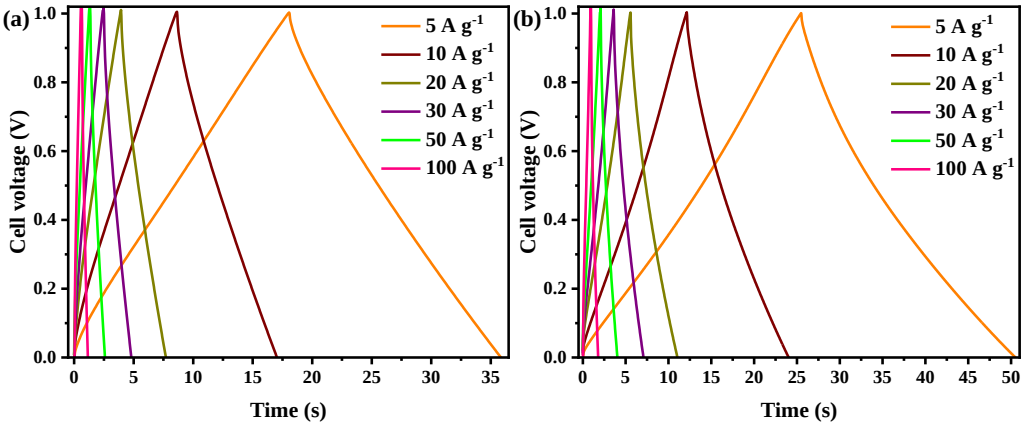

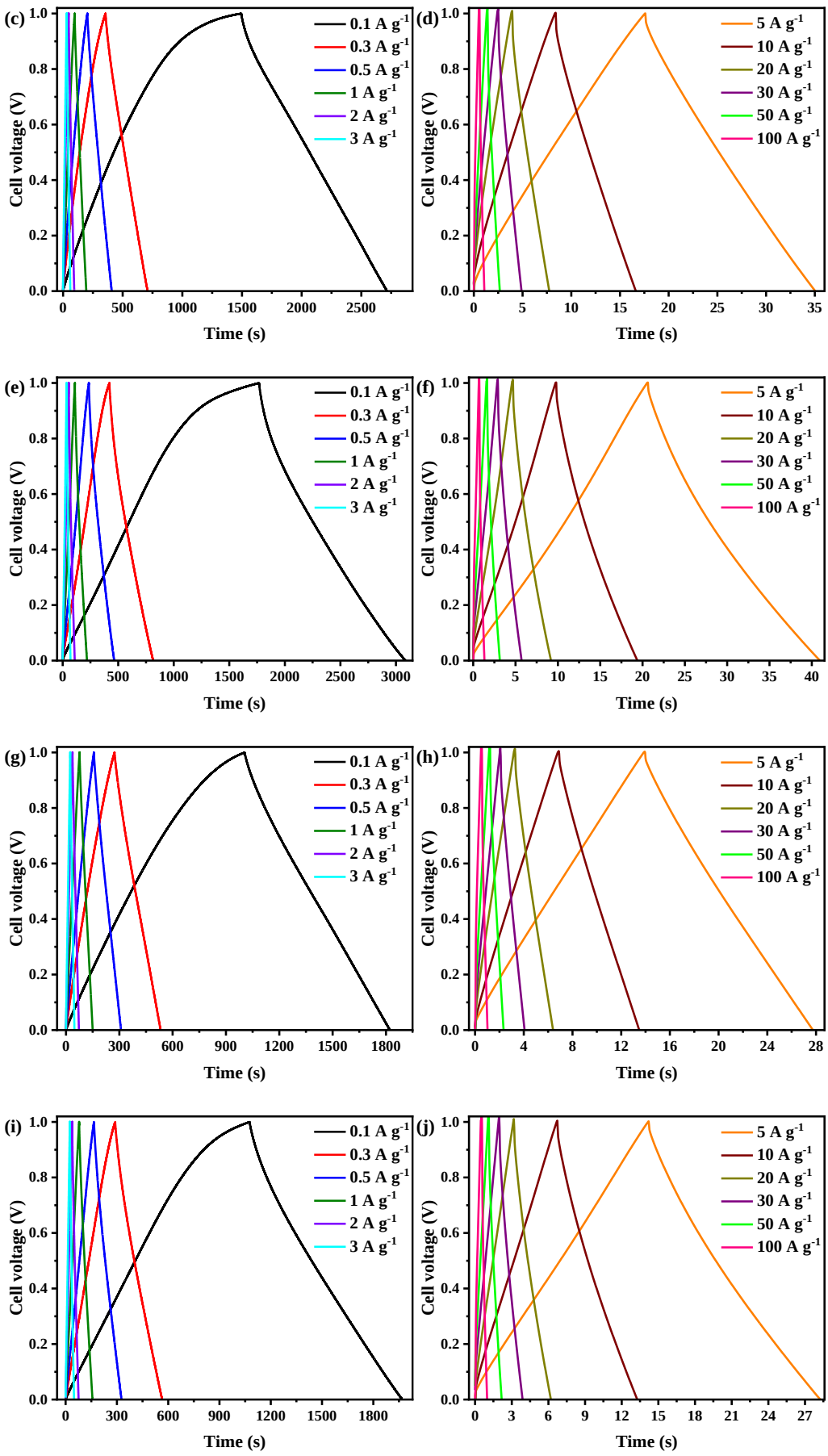
(c)
(d)
(e)
(f)
(g)
(h)
(i)
(j)
Cell voltage (V)
Time (s)
0.1 A g-1
0.3 A g-1
0.5 A g-1
1 A g-1
2 A g-1
3 A g-1
5 A g-1
10 A g-1
20 A g-1
30 A g-1
50 A g-1
100 A g-1

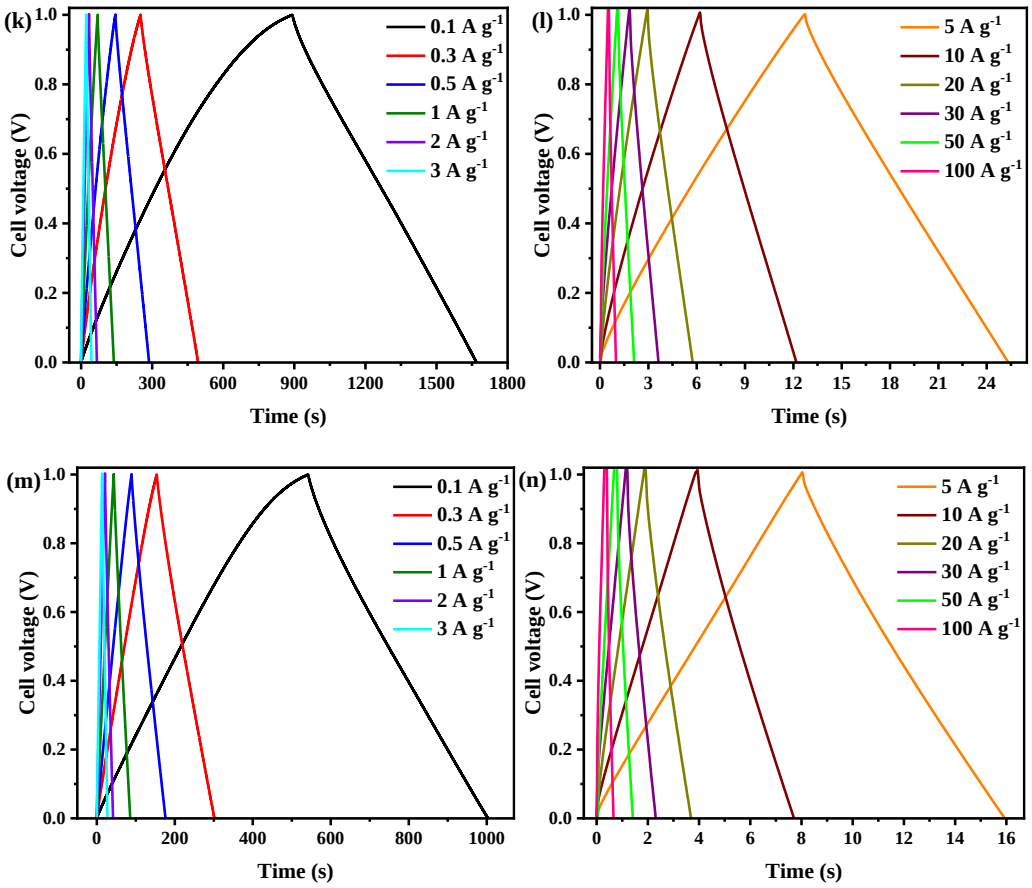

Figure S6. GCD curves of (a) NOPC-L-AS, (b) NOPC-L-AA, (c, d) NOPC-T-AS, (e, f) NOPC-T-AA, (g, h) NOPC-H-AS, (i, j) NOPC-H-AA, (k, l) OPC-G-AS and (m, n) OPC-S-AS at different current densities.

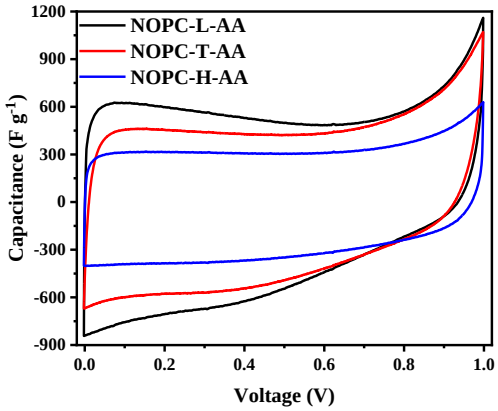

Figure S7. CV curves of NOPC-L-AA, NOPC-T-AA and NOPC-H-AA at 5 mV s^{-1}.

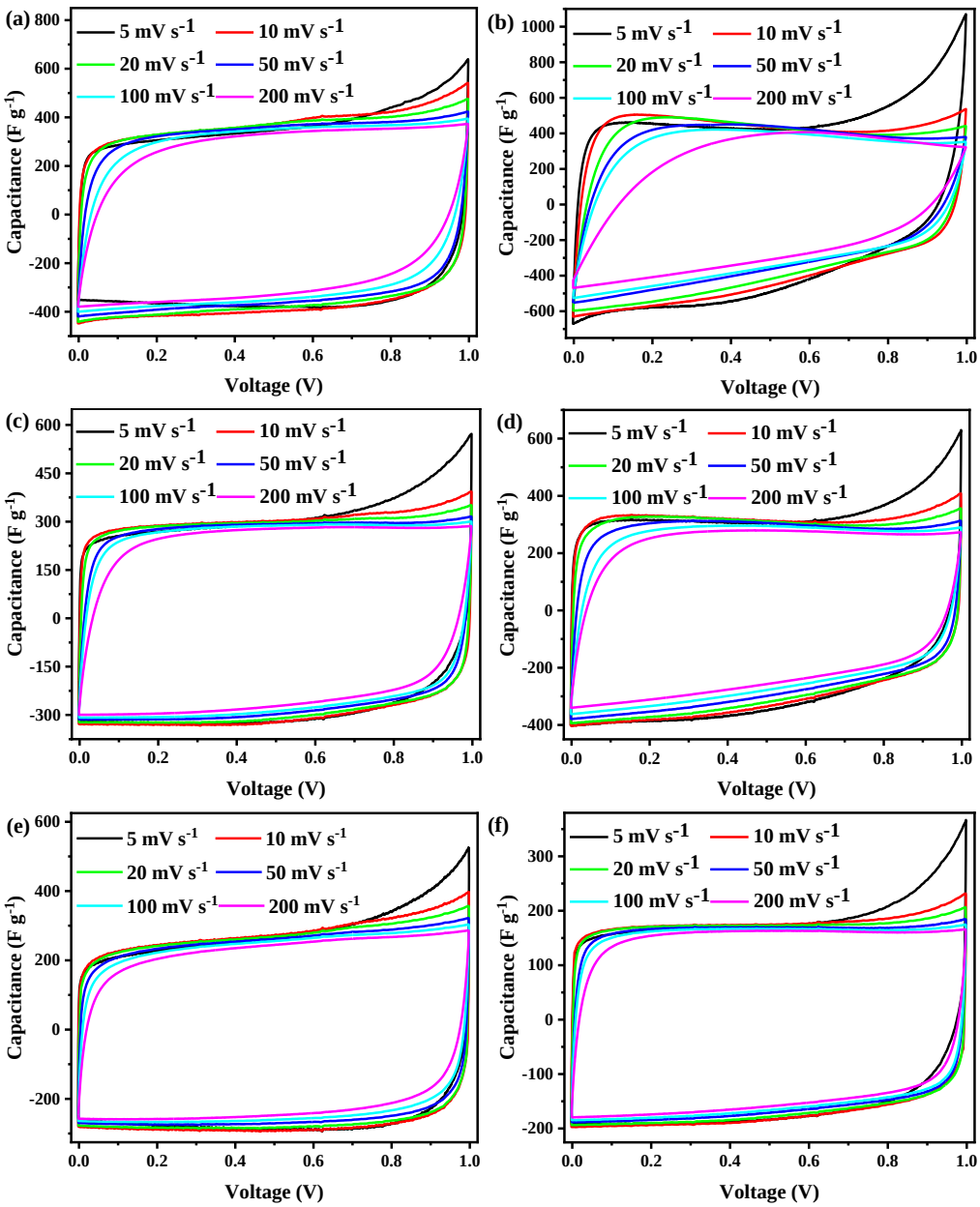

Figure S8. CV curves of (a) NOPC-T-AS, (b) NOPC-T-AA, (c) NOPC-H-AS, (d) NOPC-H-AA, (e) OPC-G-AS and (f) OPC-S-AS at different scan rates.

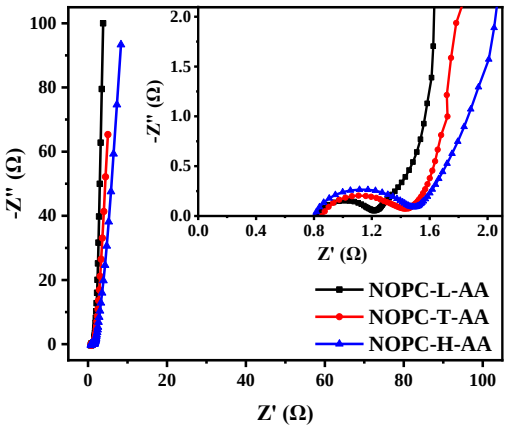

Figure S9. Nyquist plots of NOPC-L-AA, NOPC-T-AA and NOPC-H-AA.

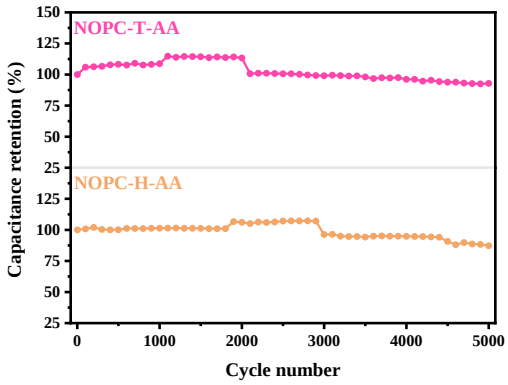

Figure S10. Cyclic stability of NOPC-T-AA and NOPC-H-AA.

Calculation process of EDLC contribution and PC contribution

Dunn method can quantitatively differentiate capacitance contribution from fast capacitive processes and diffusion-controlled Faradic processes[S1]. The fast capacitance process is closely related to EDLC, and the diffusion-controlled Faradic processes is closely related to PC. In a CV curve, the current density at a fixed potential [i(V)] can be divided into two terms, i.e.,

$$i(\mathrm{V}) = k_1 v + k_2 v^{1/2} \qquad \textbf{Equation S1}$$

where $k_1 v$ represents the current density caused by EDLC, and $k_2 v^{1/2}$ represents the current density caused by PC. Divide $v^{1/2}$ on both sides of Equation S1 to get:

$$i(\mathrm{V})/v^{1/2} = k_1 v^{1/2} + k_2 \qquad \textbf{Equation S2}$$

According to Equation S2, the relationship between $i(\mathrm{V})/v^{1/2}$ and $v^{1/2}$ is linear. Read the $i(\mathrm{V})$ at different scan rates, and fit $i(\mathrm{V})/v^{1/2}$ and $v^{1/2}$ to get k_1 and k_2. Figure S10 shows a plot of $i(\mathrm{V})/v^{1/2}$ vs. $v^{1/2}$ of NOPC-H-AS at a potential of 0.5V. The current density caused by EDLC and the current density caused by PC can be obtained by substituting k_1 and k_2 into Equation S1. Repeat for other potentials in the CV curve. The EDLC contribution and PC contribution are calculated by integrating the area of the regions. Figure S11a-c show the capacitance contribution of NOPC-H-AS, NOPC-H-AA and OPC-S-AS at a scan rate of 20 mV s^{-1}.

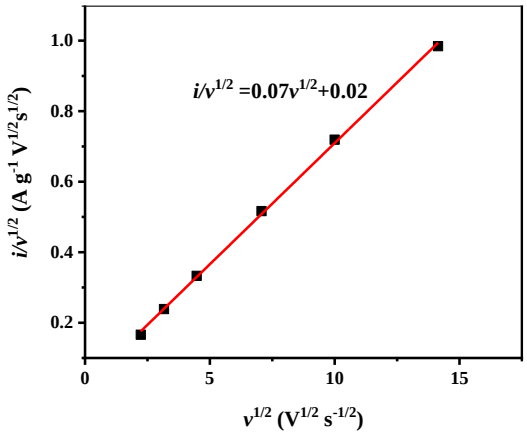

Figure S11. A plot of $i/v^{1/2}$ vs. $v^{1/2}$ of NOPC-H-AS at a potential of 0.5 V.

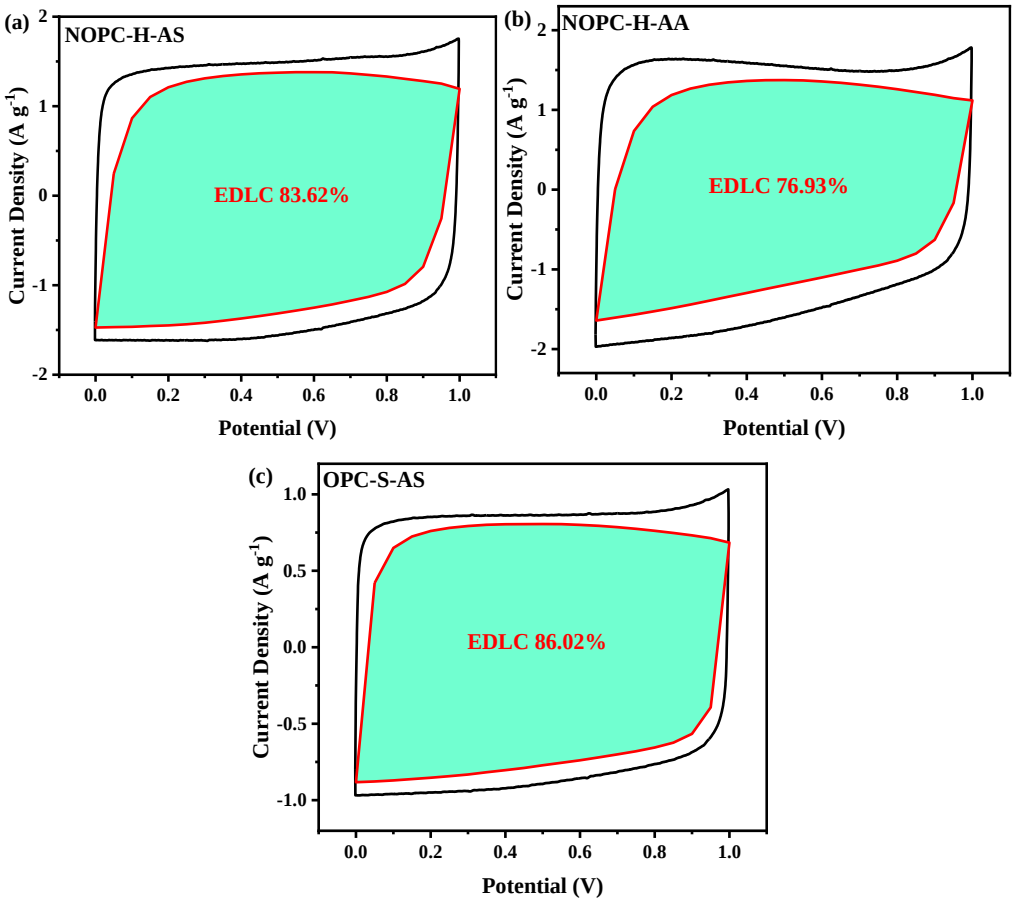

Figure S12. The capacitance contribution of (a) NOPC-H-AS, (b) NOPC-H-AA and (c) OPC-S-AS at a scan rate of 20 mV s^{-1}.

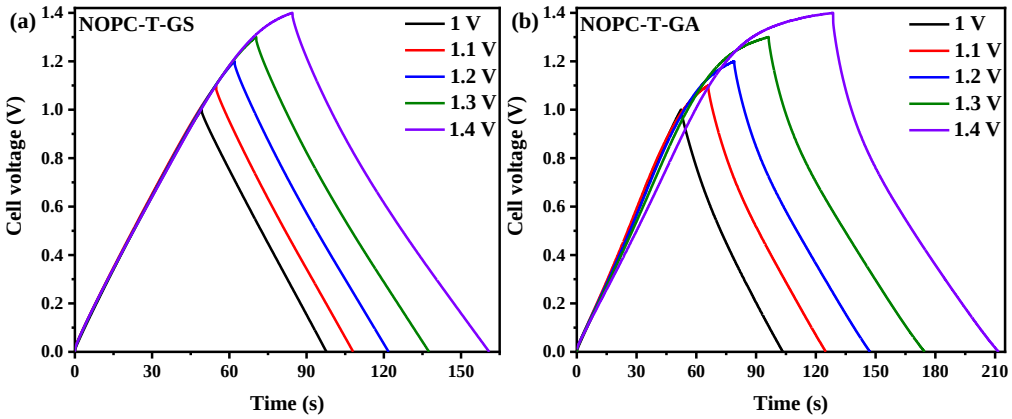

Figure S13. GCD curves of (a) NOPC-T-GS and (b) NOPC-T-GA at different voltages.

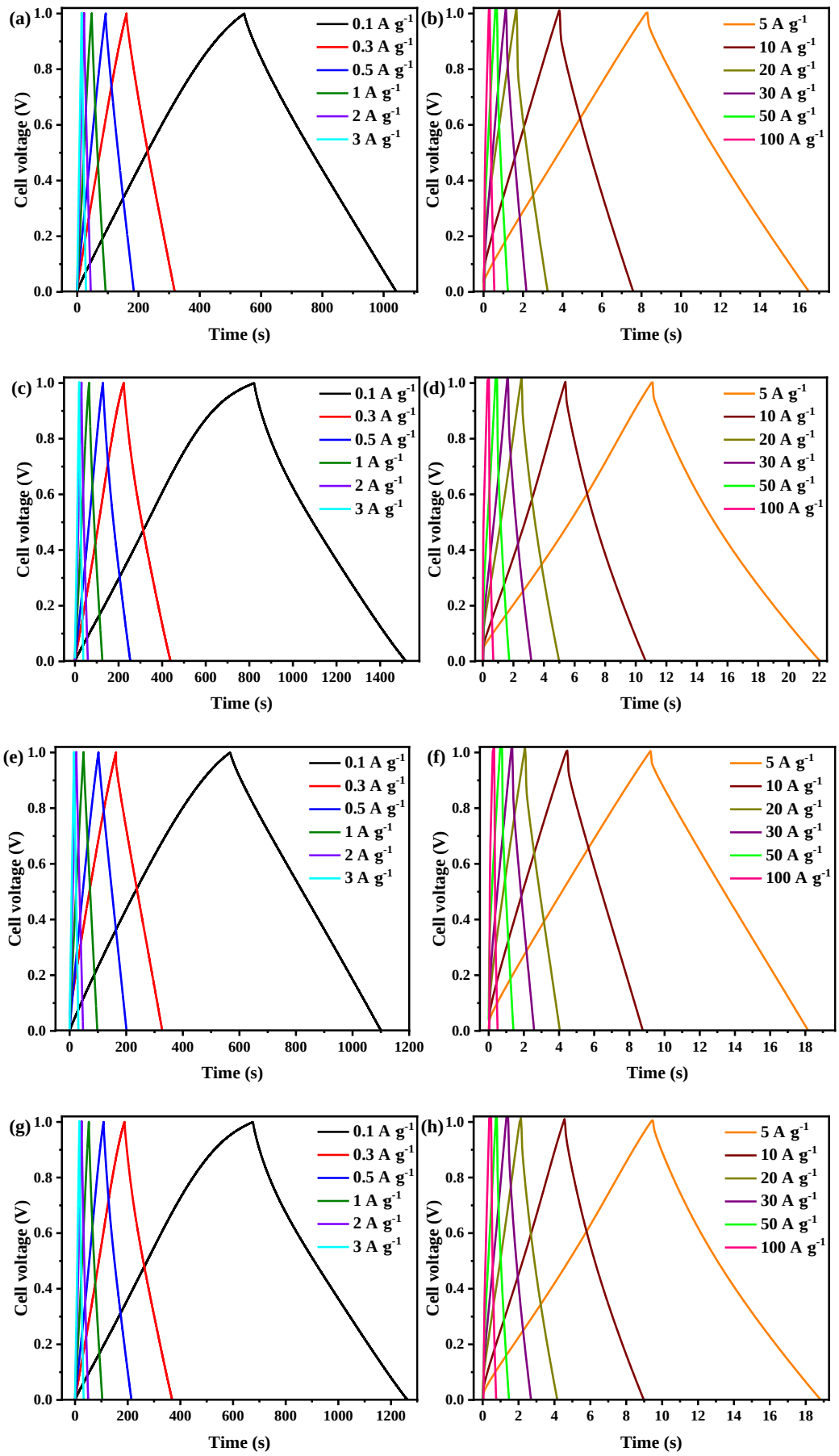
(a)
(b)
(c)
(d)
(e)
(f)
(g)
(h)
Cell voltage (V)
Time (s)
0.1 A g-1
0.3 A g-1
0.5 A g-1
1 A g-1
2 A g-1
3 A g-1
5 A g-1
10 A g-1
20 A g-1
30 A g-1
50 A g-1
100 A g-1

Figure S14. GCD curves of (a, b) NOPC-L-GS, (c, d) NOPC-L-GA,(e, f) NOPC-T-GS and (g, h) NOPC-T-GA at different current densities.

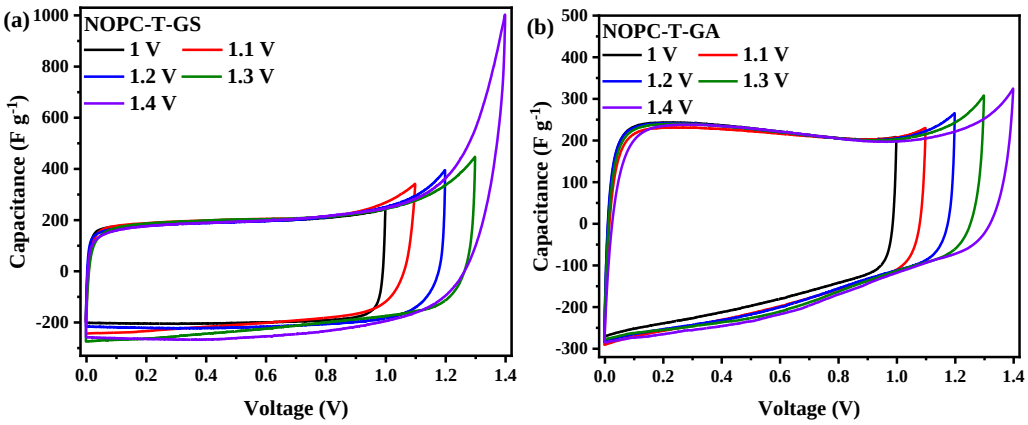

Figure S15. CV curves of (a) NOPC-T-GS and (b) NOPC-T-GA at different voltages.

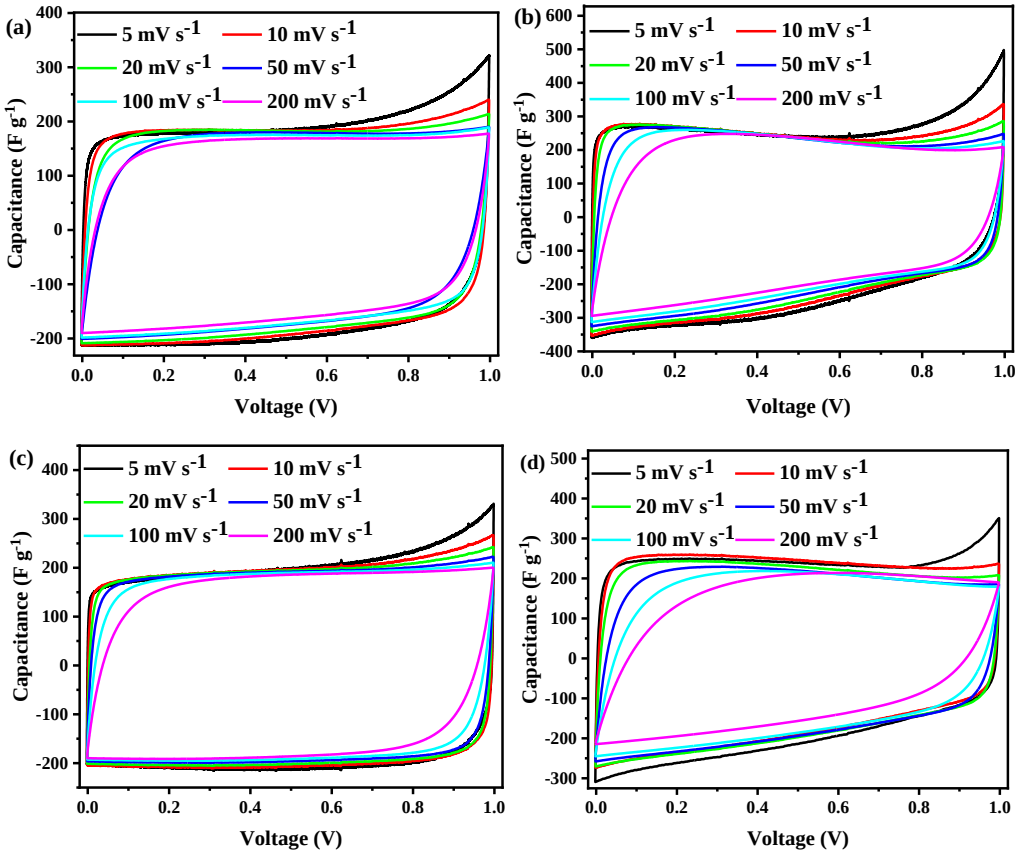

Figure S16. CV curves of (a) NOPC-L-GS, (b) NOPC-L-GA,(c) NOPC-T-GS and (d) NOPC-T-GA at different scan rates.

Table S2. Specific capacitance of the HPCs at different current densities.

Current density（A g^{-1}）		0.1	0.3	0.5	1	2	3
Capacitance ($F\ g^{-1}$)	NOPC-L-AS	514.78	439.11	419.39	399.40	380.66	373.41
	NOPC-L-AA	655.45	586.58	569.53	551.13	532.60	523.04
	NOPC-L-GS	199.46	191.07	187.39	183.25	177.27	174.83
	NOPC-L-GA	279.15	258.70	252.57	246.77	239.01	235.67
	NOPC-T-AS	489.08	424.27	409.98	393.18	377.17	370.51
	NOPC-T-AA	528.65	476.68	463.18	447.50	435.56	428.82
	NOPC-T-GS	213.63	204.34	199.23	195.78	192.34	190.23
	NOPC-T-GA	234.90	218.13	212.91	205.78	200.25	196.77
	NOPC-H-AS	327.24	311.66	306.28	297.13	291.62	288.35
	NOPC-H-AA	357.38	330.48	323.13	314.12	303.66	298.22
	OPC-G-AS	310.96	291.76	285.11	274.75	267.40	263.07
	OPC-S-AS	184.62	177.60	174.79	169.87	166.42	164.36
Current density（A g^{-1}）		5	10	20	30	50	100
Capacitance ($F\ g^{-1}$)	NOPC-L-AS	362.71	349.65	323.88	308.00	288.70	265.57
	NOPC-L-AA	512.25	495.90	475.85	466.82	463.32	457.40
	NOPC-L-GS	170.09	162.55	156.95	140.67	138.08	131.87
	NOPC-L-GA	230.27	222.89	219.95	216.69	210.64	208.80
	NOPC-T-AS	359.70	350.11	331.67	323.04	304.07	291.36
	NOPC-T-AA	419.32	407.48	392.81	387.13	375.50	373.59
	NOPC-T-GS	185.70	183.25	178.20	173.39	171.43	157.96
	NOPC-T-GA	192.00	183.86	175.64	167.86	165.55	164.72
	NOPC-H-AS	283.02	273.20	266.23	263.20	258.63	257.18
	NOPC-H-AA	289.56	276.95	262.78	258.71	249.06	241.04
	OPC-G-AS	256.71	244.84	233.67	228.15	217.98	210.61
	OPC-S-AS	161.36	156.58	151.59	150.20	145.75	144.56

Supplementary Reference

[S1] Wang, J.; Polleux, J.; Lim, J.; Dunn, B. Pseudocapacitive Contributions to Electrochemical Energy Storage in TiO2 (Anatase) Nanoparticles. *J. Phys. Chem. C* **2007**, *111*, 14925–14931.